Introduction to Theoretical Surface Science

Axel Groß
Abteilung Theoretische Chemie
Universität Ulm
Albert-Einstein-Allee 11
D-89069 Ulm
GERMANY

email: axel.gross@uni-ulm.de

Abstract

Recent years have seen a tremendous progress in the microscopic theoretical treatment of surfaces and processes on surfaces. While some decades ago a phenomenological thermodynamic approach was dominant, a variety of surface properties can now be described from first principles, i.e. without invoking any empirical parameters. Consequently, the field of theoretical surface science is no longer limited to explanatory purposes only. It has reached such a level of sophistication and accuracy that reliable predictions for certain surface science problems have become possible. Hence both experiment and theory can contribute on an equal footing to the scientific progress.

In this lecture, the theoretical concepts and computational tools necessary and relevant for theoretical surface science will be introduced. A microscopic approach towards the theoretical description of surface science will be presented. Based on the fundamental theoretical entity, the Hamiltonian, a hierarchy of theoretical methods will be introduced in order to describe surface structures and processes at different length and time scales. But even for the largest time and length scales, all necessary parameters will be derived from microscopic properties.

1 Introduction

It is the aim of theoretical surface science to contribute significantly to the fundamental understanding of the underlying principles that govern the geometric and electronic structure of surfaces and the processes occuring on these surfaces such as growth of surface layers, gas-surface scattering, friction or reactions at surfaces [1]. Processes on surfaces are play a tremendous technological role since every device interacts with the environment through its surface. Some processes at surfaces are very beneficial. For example, chemical reactions can be enormously facilitated at the surface of a catalyst. Some processes at surfaces, however, are harmful, such as corrosion or also friction.

On the experimental side, modern surface science is characterized by a broad variety of tools with microscopic resolution, the most prominent being the scanning tunneling microscope (STM) [2] which allows to image single atoms of a surface. Integrating techniques based on scattering such

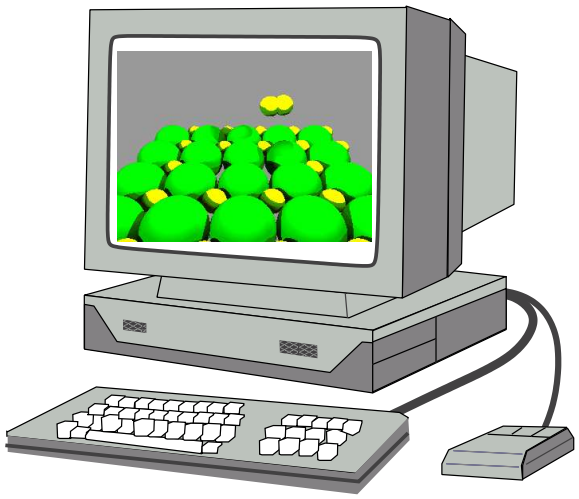

Figure 1: Simulation of surface structures and processes at surfaces on the computer.

as low energy electron diffraction (LEED) also give precise information about atomic positions on surfaces. As far as theory is concerned, while some decades ago theory could more or less only give qualitative explanations for surface science problems, the considerable improvement of computer power and the development of efficient algorithms have made it possible to describe many surface properties qualitatively and even quantitatively from first principles, i.e. without invoking any empirical parameters. It is true that the solution of the theoretical problems requires a computational approach. However, this approach is advanced enough that computational surface science may act as a virtual chemistry and physics lab at surfaces (see Fig. 1). Hence there is now a very fruitful give-and-take situation between experiment and theory with theory also being able to make reliable predictions [3].

In this chapter, I will give an introduction into the current status of theoretical surface science based on electronic structure theory. I will follow a hierarchical approach. First the basic theoretical entity, the Hamiltonian, will be discussed, and then methods to solve the corresponding Schrödinger equation will be introduced on microscopic properties. Using prototypical examples, I will give an overview over the geometric and electronic structure of surfaces and the interaction of molecules with surfaces.

2 The Hamiltonian

In solid state physics as well as in chemistry, the fundamental particles are nuclei and electrons interacting with each other through electrostatic forces. Neglecting relativistic and magnetic effects, the Hamiltonian describing a system of nuclei and electrons is given by

$$H = T_{\mathrm{nucl}} + T_{\mathrm{el}} + V_{\mathrm{nucl-nucl}} + V_{\mathrm{nucl-el}} + V_{\mathrm{el-el}}\,, \tag{1}$$

where T_{nucl} and T_{el} are the kinetic energy of the nuclei and the electrons, respectively, and the other terms describe the electrostatic interaction between the positively charged nuclei and the

electrons. Explicitly, the single terms are

$$T_{\mathrm{nucl}} = \sum_{I=1}^{L} \frac{\mathbf{P}_I^2}{2M_I}\,, \qquad T_{\mathrm{el}} = \sum_{i=1}^{N} \frac{\mathbf{p}_i^2}{2m}\,, \tag{2}$$

and

$$V_{\mathrm{nucl-nucl}} = \frac{1}{2}\sum_{I\neq J} \frac{Z_I Z_J e^2}{|\mathbf{R}_I - \mathbf{R}_J|}\,, \quad V_{\mathrm{nucl-el}} = -\sum_{i,I} \frac{Z_I e^2}{|\mathbf{r}_i - \mathbf{R}_I|}\,, \quad V_{\mathrm{el-el}} = \frac{1}{2}\sum_{i\neq j} \frac{e^2}{|\mathbf{r}_i - \mathbf{r}_j|}\,. \tag{3}$$

Here, atomic positions are denoted by capital letters, and CGS-Gaussian units have been used. In principle, we could stop here because all what is left to do is to solve the many-body Schrödinger equation using the Hamiltonian (1)

$$H\Phi(\mathbf{R},\mathbf{r}) = E\Phi(\mathbf{R},\mathbf{r})\ , \tag{4}$$

taking the proper quantum statistics such as the Pauli principle for the electrons into account. Unfortunately, the solution of the Schrödinger equation (4) in closed form is not possible, except for textbook examples such as the harmonic oscillator or the hydrogen atom. In order to solve this Schrödinger equation, a hierarchy of approximations is necessary. Usually the first approximation is the Born–Oppenheimer or adiabatic approximation [4] which is based on the separation in the time scale of processes involving electrons and atoms because of their large mass mismatch. Hence one assumes that the electrons follow the motion of the nuclei almost instantaneously.

In practice, one splits up the full Hamiltonian and defines the electronic Hamiltonian H_{el} for fixed nuclear coordinates $\{\mathbf{R}\}$ as follows

$$H_{\mathrm{el}}(\{\mathbf{R}\}) = T_{\mathrm{el}} + V_{\mathrm{nucl-nucl}} + V_{\mathrm{nucl-el}} + V_{\mathrm{el-el}}\,. \tag{5}$$

The eigenvalues $E_{\mathrm{el}}(\{\mathbf{R}\})$ of the electronic Schrödinger for a given fixed configuration $\{\mathbf{R}\}$ of the nuclei

$$H_{\mathrm{el}}(\{\mathbf{R}\})\Psi(\mathbf{r},\{\mathbf{R}\}) = E_{\mathrm{el}}(\{\mathbf{R}\})\Psi(\mathbf{r},\{\mathbf{R}\})\,. \tag{6}$$

then define the Born–Oppenheimer energy surface which acts as the potential for the nuclear motion. It is important to realize that within the Born-Oppenheimer approximation electronic excitations and electronically non-adiabatic effects are entirely suppressed. In order to describe these processes, one has to go beyond the Born-Oppenheimer approximation.

The electronic Schrödinger equation (6) is still complex enough that its solution is not trivial. As indicated in Fig. 1, in surface science one typically deals with systems where a finite object, a molecule, is interacting with a semi-infinite substrate whose ideal three-dimensional periodicity is broken in one direction. Historically, quantum chemists were the first to treat surfaces theoretically describing the surface in the cluster approach as a big molecule with wave-function based methods. In recent years, periodic calculations using density functional theory (DFT) [5] have become dominant in this field since their computational effort scales much more favorably with system size than wave-function based methods.

Before addressing methods to solve the electronic Schrödinger equation in more detail, we will first discuss the symmetry properties of surfaces. This is directly relevant for solving the Schrödinger

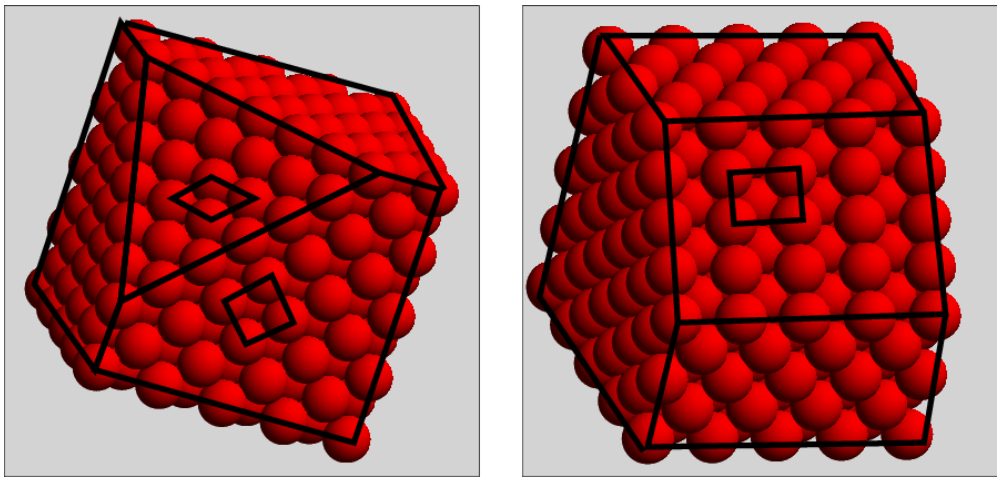

Figure 2: Structure of surfaces. Left panel: fcc crystal with (100) faces and one (111) face, right panel: fcc crystal with (100) faces and one (110) face. The surface unit cells of the corresponding faces are also indicated in the figure.

equation since every symmetry present in the Hamiltonian reduces the required computational effort significantly. Furthermore, thereby we will also introduce the notation used for the characterization of surfaces. The periodicity of a crystal lattice leads to the existence of the *reciprocal space* which reflects the translational symmetry of a lattice. Its lattice vectors are defined by

$$\mathbf{b}_1 = 2\pi \frac{\mathbf{a}_2 \times \mathbf{a}_3}{|\mathbf{a}_1 \cdot (\mathbf{a}_2 \times \mathbf{a}_3)|} \ . \tag{7}$$

where the $\mathbf{a}_i$ are the basis vectors of the real space. The other two basis vectors of the reciprocal lattice $\mathbf{b}_2$ and $\mathbf{b}_3$ are obtained by a cyclic permutation of the indices in (7). By construction, the lattice vectors of the real space and the reciprocal lattice obey the relation

$$\mathbf{a}_i \cdot \mathbf{b}_j = 2\pi\delta_{ij} \ , \tag{8}$$

where δ_{ij} is the Kronecker symbol. Further details can be found in any textbook about solid state physics [6, 7].

A surface can be thought as being created by just cleaving an infinite crystal along one surface plane. A bulk-terminated surface, i.e. a surface whose configuration has not changed after cleavage, is called an *ideal* surface. Surface planes in a crystal are denoted by the so-called *Miller indices* hkl which are defined through the shortest reciprocal lattice vector $h\mathbf{b}_1 + k\mathbf{b}_2 + h\mathbf{b}_3$ that is perpendicular to the particular plane. In Fig. 2, a fcc crystal with (100) faces is shown which have a square symmetry. Furthermore, a (111) face with a hexagonal symmetry and a (110) face with a rectangular symmetry are created by additional cuts. Together with the centered rectangular and the oblique lattices these symmetry types form the five possible two-dimensional Bravais lattices.

It is important to realize that there is no surface that remains ideal. This is due to the fact that at the surface compared to the periodic bulk there are nearest-neighbor atoms missing so that the bonding situation is changed. If the atoms at the surface just change there position

vertically without altering the surface symmetry, the surface is called to be *relaxed*. If, however, the rearrangement of the surface atoms changes the symmetry and periodicity of the surface, the surface is called to be *reconstructed*.

The symmetry of the surface of course also enters the Hamiltonian. It is always advantageous to take into account all symmetries of the Hamiltonian since only states that belong to a particular irreducible representation of the symmetry group of the Hamiltonian couple to each other through the Hamiltonian. One consequence of the existence of the two-dimensional periodicity along the surface is that the Bloch theorem is applicable in two dimensions. This means that the electronic single-particle wave functions form two-dimensional Bloch states

$$\psi_{\mathbf{k}_\parallel}(\mathbf{r}) = e^{i\mathbf{k}_\parallel \cdot \mathbf{r}} u_{\mathbf{k}_\parallel}(\mathbf{r}) \ , \tag{9}$$

where $u_{\mathbf{k}_\parallel}(\mathbf{r})$ has the two-dimensional periodicity of the surface.

3 Electronic structure calculations

The first calculations of surface structures were done by quantum chemists in the cluster approach in which the surface is regarded as a big molecule and not as an infinite periodic structure. This ansatz is guided by the idea that bonding on surfaces is a local process. However, these wave-function based calculations become prohibitively expensive for larger systems. Furthermore, this cluster approach is not really reliable for the description of extended electronic state [8] as present in, e.g., metals.

Nowadays, electronic structure calculations dealing with surfaces are predominantly performed in the framework of density functional theory (DFT) [9, 10]. They offer a good compromise between computational efficiency and sufficient accuracy for many systems. DFT can be regarded as an extension of the Thomas-Fermi theory [11] to inhomogeneous situations [9]. It is based on the Hohenberg-Kohn theorem which states that the exact ground-state density and energy can be determined by the minimization of the energy functional $E[n]$,

$$E_{\mathrm{tot}} = \min_{n(\mathrm{r})} E[n] = \min_{n(\mathbf{r})} (T[n] + V_{\mathrm{ext}}[n] + V_{\mathrm{H}}[n] + E_{\mathrm{xc}}[n]) \ . \tag{10}$$

From the Hohenberg-Kohn theorem also follows that there is a one-to-one correspondence between the electron ground-state density $n(\mathbf{r})$ and the external potential $v_{ext}(\mathbf{r})$. $V_{\mathrm{ext}}[n]$ and $V_H[n]$ are the functionals of the external potential and of the classical electrostatic interaction energy, respectively, while $T[n]$ is the kinetic energy functional for non-interacting electrons. All quantum mechanical many-body effects are contained in the so-called *exchange-correlation* functional $E^{\mathrm{xc}}[n]$, which is an universal functional of the density, i.e., it does not depend on any particular element, but unfortunately it is not known in general.

Since the kinetic energy functional $T[n]$ is not precisely known for inhomogeneous situations, the Hohenberg-Kohn theorem is not useful for a direct implementation of the DFT (however, there is recently a renewed interest in so-called orbital-free DFT calculations [12]). Instead, one expresses

the electron density $n(\mathbf{r})$ as the sum over so-called single-particle Kohn-Sham states

$$n(\mathbf{r}) = \sum_{i=1}^{N} |\psi_i(\mathbf{r})|^2 \ , \tag{11}$$

which are obtained by a self-consistent solution of a set of coupled effective one-particle equations, the Kohn-Sham equations [10]

$$\left\{ -\frac{\hbar^2}{2m}\nabla^2 + v_{ext}(\mathbf{r}) + v_{\rm H}(\mathbf{r}) \ + \ v_{\rm xc}(\mathbf{r}) \right\} \ \psi_i(\mathbf{r}) = \varepsilon_i \ \psi_i(\mathbf{r}) \ , \tag{12}$$

where $v_{\rm ext}$ is the external potential. The *Hartree potential* $v_{\rm H}$ is given by

$$v_{\rm H}(\mathbf{r}) = \int d^3\mathbf{r}' n(\mathbf{r}') \frac{e^2}{|\mathbf{r}-\mathbf{r}'|} \ . \tag{13}$$

Furthermore, the exchange-correlation potential $v_{\rm xc}(\mathbf{r})$ is the functional derivative of the exchange-correlation functional $E_{\rm xc}[n]$

$$v_{\rm xc}(\mathbf{r}) = \frac{\delta E_{\rm xc}[n]}{\delta n} \ . \tag{14}$$

The ground state energy can then be expressed as

$$E = \sum_{i=1}^{N} \ \varepsilon_i + E_{\rm xc}[n] - \int v_{\rm xc}(\mathbf{r}) n(\mathbf{r}) \ d^3\mathbf{r} - V_{\rm H} \ . \tag{15}$$

The first term in the total-energy expression (15) is also called the band structure term $E_{\rm bs}$ since it corresponds to the sum over the single-particle energies. The Kohn-Sham equations have to be solved iteratively in a self-consistent scheme since the solutions of the Kohn-Sham equations also enter the effective one-particle Hamiltonian. Initially the electron density is guessed, for example as a superposition of atomic densities. The Kohn-Sham equations are then solved and the resulting density is compared to the initial guess. If the difference is larger than some pre-specified value, the new density enters the Kohn-Sham equations (often using some mixing scheme), and the cycle is repeated so often until the iterations no longer modify the solutions, i.e. until self-consistency is reached.

In principle, DFT provides an exact expression of the total energy. Unfortunately, this is of no great practical advantage since the correct form of the non-local exchange-correlation functional and the related exchange-correlation potential v_{xc} is not known. Therefore, approximative expressions are needed. For bulk situations, the local density approximation (LDA), in which at any position $\mathbf{r}$ the exchange-correlation potential of the homogeneous electron gas with the corresponding electron density is used, has been surprisingly successful [13]. However, for chemical reactions at surfaces the LDA not sufficiently reliable [14]. For large scale DFT calculations of surfaces and nanostructures the so-called generalized gradient approximation (GGA) [15] represents the state of the art. In the GGA, the gradient of the density also into account in the exchange-correlation functional, but in such a way that important electronic sum rules are obeyed. The GGA yields a satisfactory accuracy for many applications, although there are still exceptions [16, 17]. There is certainly a strong need for further improvements of the exchange-correlation functionals.

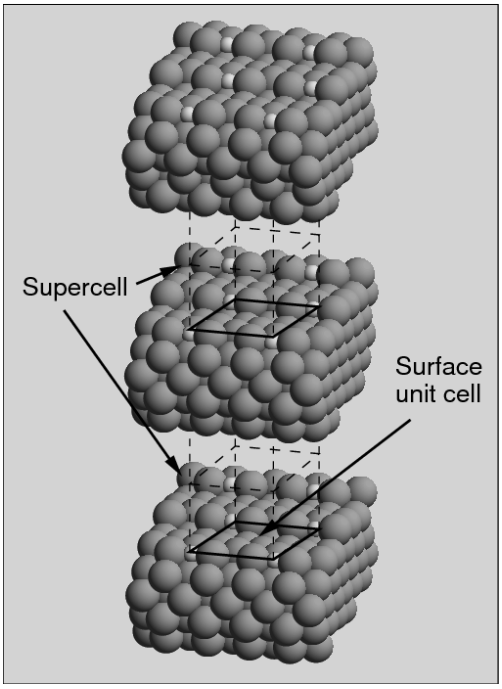

Figure 3: Illustration of the supercell approach. A substrate of a fcc crystal with a (410) surface termination and an adsorbed periodic atomic layer in a (2×1) geometry is represented by an infinite array of slabs. The supercell and the surface unit cell are indicated in the figure.

It is numerically very efficient to use a plane-wave expansion of the Kohn-Sham single-particle states, but such an approach usually requires a three-dimensional periodicity of the considered system. Still, plane-wave codes can be used to model surface problems in the so-called supercell approach: the surfaces are modeled by periodically repeated slabs. In Fig. 3, a typical supercell describing the adsorption of atoms at the step sites of a nanostructured fcc(410) surface in a (2×1) geometry is shown. The slabs have to be thick enough to reproduce the correct electronic structure of the substrate, and they have to be separated enough in order to avoid any interaction between the slabs. One advantage of the slab approach is that the substrates are infinitely extended in lateral directions which yields a correct description of the delocalized nature of the electronic states of metals, a feature that is not present when the substrate is modeled by finite clusters [8].

4 Electronic and geometric structure of surfaces

At a surface of a solid, the electronic structure is strongly modified with respect to the bulk electronic structure. Although the periodicity parallel to the surface is conserved, along the surface normal the periodicity is broken so that the wave number k_z of the Bloch waves no longer is a good quantum number. There is a very simple model which is able to illustrate some fundamental properties of the electronic structure of surfaces, in particular simple metal surfaces, namely the so-called jellium model. In this model, the positive ion charges are replaced by a uniform charge

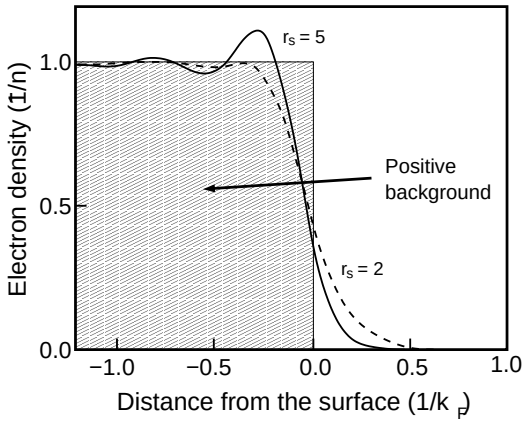

Figure 4: Charge density as a function of the distance from the surface in Fermi wavelengths determined within the jellium model for two different background densities denoted by the Wigner–Seitz radius in atomic units, i.e., in multiples of the Bohr radius (after [18]).

background,

$$n_+(\mathbf{r}) = \begin{cases} \bar{n}, & z \leq 0 \\ 0, & z > 0 \end{cases} . \tag{16}$$

Here z denotes, as usual, the direction perpendicular to the surface. The bulk charge density in the jellium model is commonly specified by the Wigner–Seitz radius

$$r_s = \left(\frac{3}{4\pi n}\right)^{1/3}, \tag{17}$$

which corresponds to the radius of the sphere whose volume $V/N = 1/n$ equals the volume per electron in the homogeneous electron gas.

Using DFT, the charge density within the jellium model has been determined for several different different bulk charge densities [18]. Two examples corresponding to a high-density ($r_s = 2$) and a low-density metal ($r_s = 5$) are shown in Fig. 4. The electron distribution does not follow the sharp edge of the positive background but rather exhibits a damped oscillatory structure inside the jellium which is stronger in the low-density case. These *Friedel oscillations* are a consequence of the sharp edge of the background density in the jellium model [1]. Furthermore, it is obvious that some electronic charge density spills out into vacuum, thereby creating a dipole layer. This dipole layer contributes to the so-called work function of the metal Φ which is defined as the minimum work that must be done to remove an electron from a solid at 0 K.

The jellium model has been used to evaluate the work function of simple and noble metals [19] which is typically in the range of 2 to 5 eV. For simple *sp*-bonded metals such as Na, K or Cs with rather delocalized electron orbitals, the jellium model is surprisingly successful, however, for metals with *d* electrons which are much more localized the jellium model is no longer appropriate. Furthermore, the jellium model can also not describe the occurrence of surface states which are electronic states localized near the surface. These states are a consequence of a band gap in the projected bulk band structure which allows for metal states that are delocalized parallel to the surface but decay exponentially into the bulk.

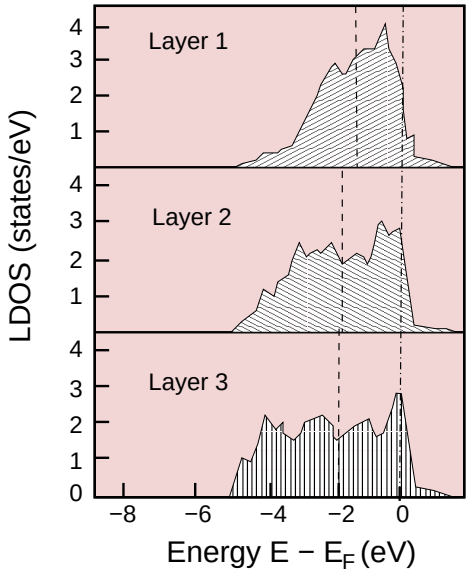

Figure 5: Layer-resolved, local d-band density of states of Pd(210) determined by GGA-DFT calculations. The Fermi level and the center of the d-band are indicated by vertical lines. The third-layer PDOS is already very close to the bulk density of states of palladium (after [23]).

Furthermore, at a surface the local density of states (LDOS)

$$n(\mathbf{r}, \varepsilon) \;=\; \sum_i \; |\phi_i(\mathbf{r})|^2 \; \delta(\varepsilon - \varepsilon_i) \; . \tag{18}$$

is also modified compared to the bulk. In a simple tight-binding picture, the width of an electronic band is directly related to the coordination and the overlap of the orbitals. Surface atoms have a lower coordination than bulk atoms, hence the local band width will become narrower. In fact, the same is also true for pseudomorphic overlayers under tensile strain which reduces the overlap between the electronic orbitals [20, 21, 22]). If the band is more than half-filled but not completely filled and the band center is kept fixed, the number of states below the Fermi energy will increase. This would lead to an higher occupation of the band. However, the number of electrons is conserved. In order to obey charge conservation, the narrower band has to shift up so that the number of occupied states remains unchanged.

This effect is illustrated in Fig. 5 where the results of GGA-DFT calculations concerning the layer-resolved, local d-band density of states of the stepped Pd(210) surface are shown [23]. The LDOS of the third layer is still rather similar to the Pd bulk density of states. This is due to the good screening properties of metals [6] which lead to a rapid recovery of bulk properties in the vicinity of imperfections such as surfaces. However, the width of the d-band of the second and first layer are significantly reduced, and this reduction in band width is accompanied by an upshift of the d-band centers indicated by the vertical dashed lines.

Such an upshift of the d-band has significant consequences for the reactivity which can be understood within the so-called d-band model [24, 25]. This scheme is closely related to the frontier orbital concept developed for gas-phase reactions [26, 27]. In the d-band model, the whole d-band

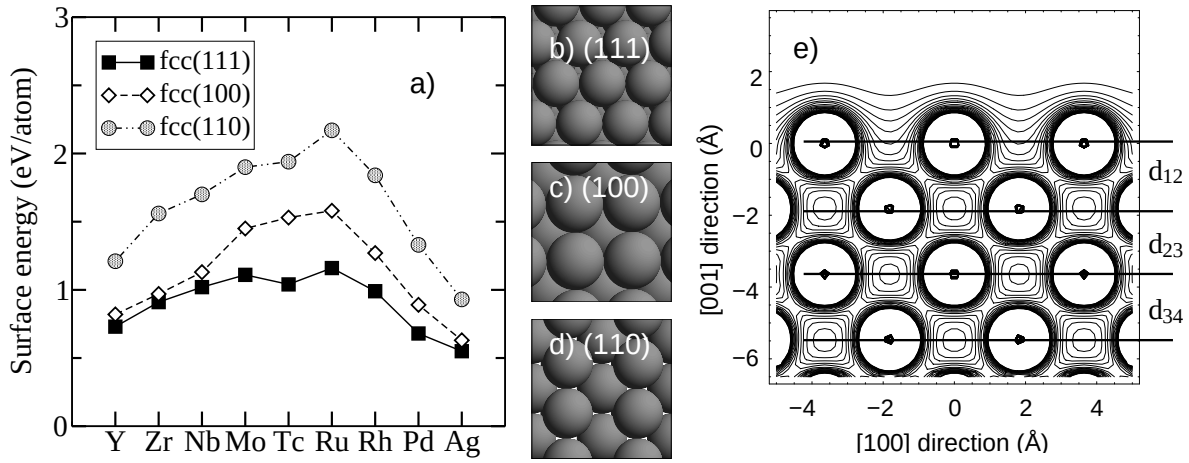

Figure 6: First-principles surface energies for the $4d$ transition metals calculated using density functional theory within the local density approximation [32]. The energies have been determined for the (111), (100) and (110) surfaces in the fcc structure even for the hcp metals Y, Zr, Tc and Ru and for the bcc metals Nb and Mo. **(a)** surface energy in eV/atom, **(b-d)** structure of the fcc (111), (100) and (110) surface, respectively; **(e)** electron density of a Cu(001) surface along a (010) plane calculated by DFT-GGA calculations [1] together with the notation of the layer spacing d_{ij}.

is replaced by an effective level located at the center of the d-band ε_d. This level then interacts with the molecular orbitals of an adsorbate. If the interaction is sufficiently strong, the molecular levels split because of the strong hybridization with the metal d-states into a bonding and an anti-bonding contribution. The closer the d-band center is to the Fermi energy, the more reactive the system usually is because the less any anti-bonding contribution is occupied. If relatively similar systems are compared which only differ in the position of the d-band center, to first order a linear relationship between the d-band center shift and the change in the chemisorption strength ΔE_d [28, 29] results,

$$\delta E_d = -\frac{V^2}{|\epsilon_d - \epsilon_a|^2}\ \delta\varepsilon_d\ , \tag{19}$$

which means that an upshift of the d-band leads to a stronger interaction or larger energy gain. This explains why low-coordinated sites such as for example step sites can exhibit a significantly higher reactivity than flat terrace sites [30, 31].

Energetically, however, stepped metal surfaces are unfavorable. In fact, the more densely packed a certain lattice plane and the higher coordinated the atoms in that plane, the less bonds have to be broken upon cleavage. Hence the most densely packed surface should have the lowest surface energy. This is indeed the case for almost all $3d$, $4d$ and $5d$ transition metals. We have illustrated this trend in Fig. 6 where calculated surface energies for the fcc(111), (100) and (110) termination of the $4d$ transition metals are plotted in eV/atom [32] together with an illustration of their structure. The densely packed (111) surfaces with their ninefold coordinated surface atoms have the lowest surface energy per atom, i.e. they correspond to the most stable structure, while the more open (100) surfaces (eightfold coordination) and the (110) (sixfold coordination) are less stable.

Figure 6 also indicates the chemical trend in the surface energies. There is a parabolic shape of the

surface energies as a function of the d-band occupation. In order to make this dependence more obvious, all surface energies have been calculated for the fcc structure, even for the hcp metals Y, Zr, Tc and Ru and for the bcc metals Nb and Mo. The surface energies are maximal for a half-filled d-band, while they are minimal for either an empty or a completely filled d-band. The same trend is also observed for the 3d and the 5d transition metals [33] and is already well-known for the cohesive energies [6]. The relationship between the cohesive and the surface energies can be made quantitative within the so-called bond-cutting model which takes into account that the bond strength varies with the coordination number. For a low-coordinated atom the single bonds are stronger than for a high-coordinated atom.

In a simple tight-binding picture, the energy per bond can be assumed to scale with $(N_c)^{1/2}$. If we denote the surface energy per atom by σ, we can estimate it by

$$\sigma \;=\; \frac{\sqrt{N_c^{bulk}} - \sqrt{N_c^{surf}}}{\sqrt{N_c^{bulk}}}\; E'_{coh}\;, \tag{20}$$

where N_c^{bulk} and N_c^{surf} are the coordination number of the bulk and the surface, respectively, and E'_{coh} is the cohesive energy related to a *non-magnetic* atom for a non-magnetic surface. For a fcc(111) surface Eq. (20) yields a surface energy per atom of $\sigma = 0.134\, E'_{coh}$ which gives results rather close to the ones plotted in Fig. 6a.

The electron density at a metal surface is rather smooth, as illustrated in Fig. 6e. This is due to the fact that at the surface the electrons are free to lower their kinetic energy by becoming more uniformly distributed which results in the so-called Smoluchowski smoothing [34]. In addition, in Fig. 6e the notation of the layer spacing d_{ij} is introduced. For an ideal surface, the layer spacing would be the same as the bulk layer spacing. Real surfaces, however, show *relaxation* effect: due to the modified environment compared to the bulk, the layer spacing is changed. Still the changes are rather small for most metal surfaces, as is illustrated in table 1 for the low-index copper surfaces. At metal surfaces, the smoothening of the electron density usually leads to a contractive relaxation of the first layer. For the densely packed (111) and (100) Cu surfaces, this contraction is negligible, but for the more open surfaces (see Cu(110)) it can be already rather significant. Furthermore,

Table 1: Surface energies γ and relaxations of the uppermost layer of various Cu surfaces. The relaxations are given in percent relative to the bulk layer spacing d_0(hkl).

Surface	Method	γ (J/m^2)	Δd_{12}	Δd_{23}	Δd_{34}	d_0(hkl) (Å)
Cu(111)	Theory[a]	1.30	-0.9	-0.3		2.10
Cu(111)	Exp.	∼1.79[b]	-0.7[c]			
Cu(100)	Theory[a]	1.45	-2.6	1.5		1.821
Cu(100)	Exp.	∼1.79[b]	-2.1[d]	0.4[d]	0.1[d]	1.807
Cu(110)	Theory[e]	1.53	-10.8	5.3	0.1	1.29
Cu(110)	Exp.	∼1.79[b]	-8.5[f]	2.3[f]		

References: a) [35], b) [36], c) [37], d) [38], e) [39], f) [40],

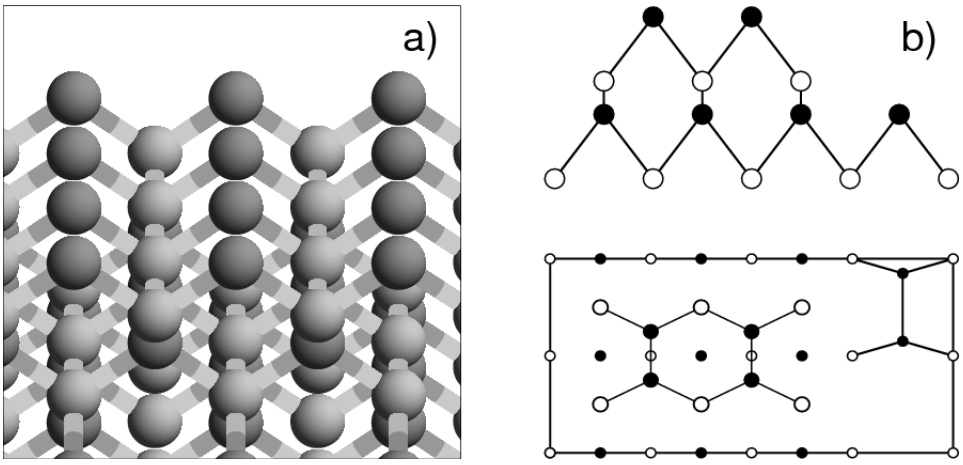

Figure 7: Structural models for the GaAs(100) surface. Dark, filled circles and bright, empty circles represent As and Ga atoms, respectively. (**a**) Ball and stick model of the ideal (1×1) As-terminated GaAs(100) surface. (**b**) Schematic top and side view of the $\beta2(2\times4)$ reconstruction. Larger circles correspond to atoms closer to the surface.

many metal substrates respond to the contraction of the first interlayer spacing by an expansion of the second interlayer, as for example the Cu(100) and (110) surfaces. However, this oscillatory behavior does not necessarily occur.

In addition, in table 1 the surface energies are included. The experimental values are derived from surface tension measurements which are made in the liquid phase and extrapolated to zero temperature [36]. This does also mean that these surface energies are not related to any particular crystal face, but it is obvious that the measured surface energy has the same order of magnitude as the calculate ones. Furthermore, for the low-index surfaces of Cu the trend $\gamma_{(111)} < \gamma_{(100)} < \gamma_{(110)}$ is confirmed.

While for the transition metals the modified bond-cutting model Eq. (20) gives a reliable estimate of the surface energies, the situation for the divalent fcc and bcc sp-metals is not that simple. For metals such as Ca, Sr or Ba the surface energies of the second most close packed surface are consistently smaller than the ones of the most closed packed surface [33]. Even more complex is the situation for semiconductor surfaces. Truly directional bonds between atoms will be broken upon cleavage which creates an highly unstable state. The surface will try to minimize the number of unsaturated bonds, the so-called dangling bonds. A prominent example of the resulting surface reconstruction is provided by the GaAs(100) surface.

The evaluation of the most stable surface structure for compound materials is more complex than for elemental materials, because the relevant entity is no longer the total energy but rather the free energy which at zero temperature is given by

$$\gamma \;=\; \frac{1}{A}\,(E_{\rm surf} \;-\; \sum_i \mu_i N_i)\;. \tag{21}$$

The chemical potentials μ reflect the specific thermodynamic conditions of the preparation of the surface, i.e., the reservoir with which the atoms are exchanged in a structural transition. For gas-

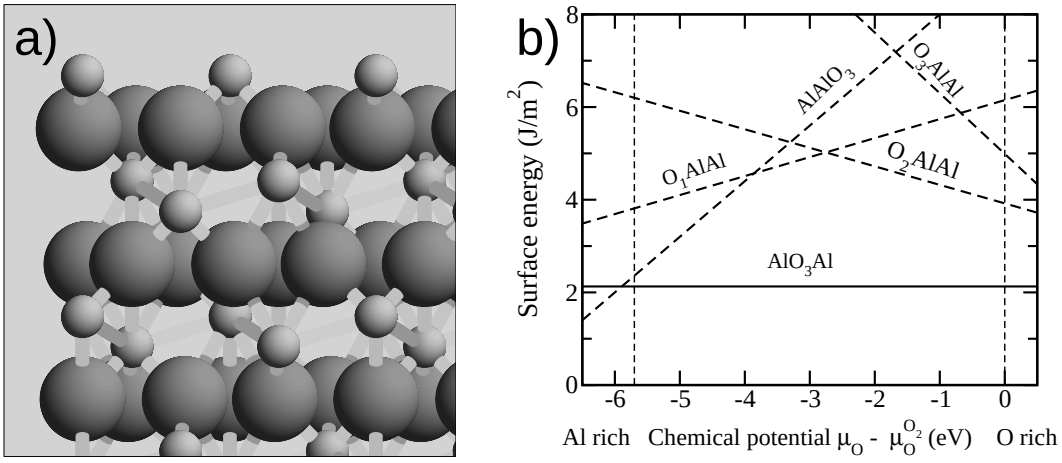

Figure 8: $Al_2O_3(0001)$ surface. a) Side view of the ideally Al-terminated surface structure showing the Al-O-Al trilayer structure. b) Surface energies of different $Al_2O_3(0001)$ (1×1) structure in J/m^2 as a function of the difference of the oxygen chemical potential (after [43]). The uppermost layers of the corresponding structures are indicated in the figure. The perpendicular lines indicate the range of possible oxygen chemical potentials.

phase deposition, they can be directly related to the partial pressure at a certain temperature. E_{surf} is the total energy of the surface per unit cell. As far as the structure of GaAs(100) is concerned, the ideal surface structure (Fig. 7a) is highly unstable because of the large number of broken bonds. The GaAs surface tries to minimize the number of dangling bonds by dimerization. Still, at the dimer atoms of a (100) surface one dangling bond per atom remains. In general, polar semiconductors exhibit surface reconstructions with the anion dangling bonds filled and the cation dangling bonds empty. This so-called *electron-counting principle* leads to a semiconducting surface since the occupation of Ga dangling bonds which are higher than As dangling bonds would result in a metallic surface which is energetically unfavorable. The $\beta 2(2\times4)$ surface structure (see Fig. 7b) fulfilling these requirements is stable over a wide range of As chemical potentials [41, 42].

Finally the structure of ionic surfaces shall be addressed. Typically alkali halide crystals in equilibrium are almost ideally terminated by non-polar surfaces without any dipole moment perpendicular to the surface. A typical example is the {100} surface of the sodium chloride structure. Since the formation of a dipole layer is energetically rather costly, polar surfaces are usually highly unstable. Because of that reason salt grains have an almost perfect cubic shape. Surface structures are more complicated for insulating oxide materials where the bonds still have a covalent character although there is a significant charge transfer between the constituents. As an example, we consider the (0001) surface of α-Al_2O_3 (corundum or sapphire) which has been studied extensively by both theory [43, 44, 45, 46] and experiment [47, 48].

α-Al_2O_3 (sapphire) crystallizes in the corundum structure that can be described by a primitive rhombohedral unit cell with two Al_2O_3 formula units, but more convenient is the hexagonal unit cell that contains 12 Al atoms and 18 O atoms. The hexagonal cell corresponds to a layered structure with six oxygen planes associated with aluminum planes above and below it, forming

stoichiometric triple Al-O-Al layers with three O atoms and just one Al atom in each layer per unit cell, as can be seen in a side view of the ideally Al-terminated α-$Al_2O_3(0001)$ surface shown in Fig. 8a. Because of this layered structure, there is no non-polar termination of the α-$Al_2O_3(0001)$ surface.

Figure 8b shows the calculated surface energies as a function of the oxygen chemical potential for different (1×1) terminations [43, 46]. These surface free energies have been determined using Eq. 21. In fact, the total energy of every surface structure has to be calculated only once, and the slope of the curves is given by the stoichiometry of the surface with respect to the bulk stoichiometry. The two perpendicular lines indicate the range of possible oxygen chemical potentials. For larger oxygen chemical potentials molecular oxygen is more stable, for smaller chemical potentials bulk Al becomes the preferred phase. Within the range of possible chemical potentials the structure with the lowest free energy is the one that is stable. According Figure 8b, over the entire range of oxygen chemical potentials the stoichiometric AlO_3Al-termination is by far the energetically most favorable one. This can be understood by simple electrostatic arguments because the triple AlO_3Al layer does not have a dipole moment while all other (1×1) surface terminations have one. However, it should be noted that there is a strong inward relaxation of the first Al-layer so that it practically becomes coplanar with the oxygen layer [43, 49]. In contrast, the interlayer spacing between the second and third layer is only slightly modified compared to the bulk spacing.

5 Interaction of atoms and molecules with surfaces

The interaction of atoms and molecules with surfaces is ubiquitous since all materials interact with their environment via their surfaces. Certain chemical reactions can be significantly accelerated at surfaces which is used in heterogeneous catalysis. However, for many devices and applications any interaction with the environment should be rather avoided. One example is the high energetic exchange between the atmosphere and rockets or high-speed missiles which causes significant temperature rises that lead to chemical reactions and particle ionizations. Hence a deeper knowledge about the principles underlying gas-surface interactions and adsorption is not only of fundamental interest, but it is also technologically very relevant.

Basically one distinguishes two kinds of adsorption at surfaces. If true chemical bonds between substrate and adsorbate are formed, it is called *chemisorption*, otherwise it is called *physisorption* which is usually much weaker. We will start by discussing the nature of physisorption.

Any molecule in front of a surface experiences an attraction towards the surface caused by the van der Waals forces, i.e., the attraction is due to the induced dipole moment interacting with its own image charges in the polarizable solid. Although this interaction is usually rather weak ($\sim 0.1\,\mathrm{eV}$), it is in fact crucial for the bonding in a wide range of matter. Although the van der Waals interaction is a quantum phenomenon, some basics about this interaction can be understood within a purely classical picture. In Fig. 9, a hydrogen atom in front of a metal surface is schematically drawn. This hydrogen atom is interacting with its image charges of both the nucleus and the electron in the conductor. If one adds up the electrostatic interaction of all charges and performs a Taylor expansion in the small parameter $|\mathbf{r}|/|\mathbf{R}|$, where $|\mathbf{R}| = Z$ and $|\mathbf{r}|$ are the atom-surface and the

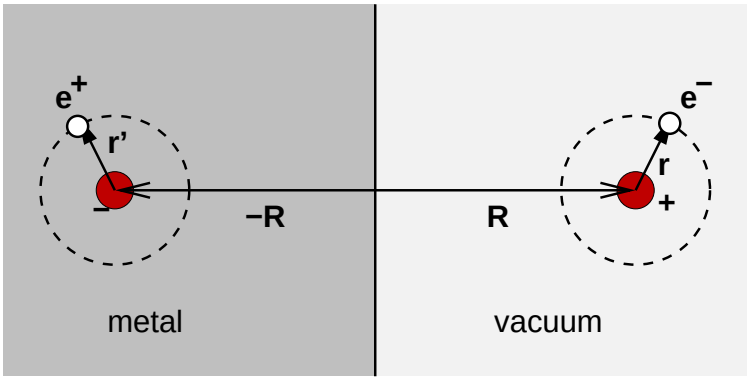

Figure 9: Van der Waals interaction: schematic illustration of a hydrogen atom in front of a perfect conductor interacting with its image charges.

proton-electron distance, respectively, one obtains

$$V_{\rm im} = -\frac{e^2}{8Z^3}\left[\frac{x^2+y^2}{2}+z^2\right] + \frac{3e^2}{16Z^4}\left[\frac{z}{2}(x^2+y^2)+z^2\right] + O(Z^{-5}) \ . \tag{22}$$

Here, x, y and z are the components of $\mathbf{r}$. Introducing the atomic polarizability

$$\alpha = \frac{e^2}{m_e\omega_{\rm vib}^2} \ . \tag{23}$$

and the van der Waals constant $C_v = \hbar\omega_{\rm vib}\alpha/8$, the electrostatic interaction can be written as

$$V_{\rm im}(Z) = -\frac{C_v}{Z^3} - \frac{3C_vZ_0}{Z^4} + O(Z^{-5}) = -\frac{C_v}{(Z-Z_0)^3} + O(Z^{-5}) \tag{24}$$

where Z_0 is the so-called *dynamical image plane*. This expression confirms the long-range nature of the van der Waals interaction which is proportional to Z^{-3}. In this derivation, we have treated the hydrogen atom as a dipole interacting with its image dipole at a distance $2Z$. However, a hydrogen atom in the ground state has no permanent dipole moment. Therefore a rigorous quantum mechanical derivation of the long-range interaction between a neutral atom and a solid surface is necessary. Still, such a quantum treatment results in an analogous expression as Eq. (24) with the van der Waals constant also basically proportional to the polarizability of the atom [50].

The attractive van der Waals force is always present for any molecule interacting with surfaces, but if close to the surface true chemical bonds are formed, then the additional, relatively weak van der Waals interaction is negligible. Only for inert atoms and molecules with closed valence shells such as the noble gas atoms, the van der Waals interaction is the main source of binding to the surface. Close to the surface, the molecular wave functions start to overlap with the substrate orbitals. Because of the Pauli principle the wave functions have to be orthogonal to each other leading to the short-range Pauli repulsion. The balance between the short-range Pauli repulsion and the long-range van der Waals attraction leads to the existence of a physisorption minimum. Figure 10 shows the physisorption potential for He interaction with jellium surfaces with densities corresponding to Ag, Cu and Au where the Pauli repulsion has been evaluated using Hartree–Fock

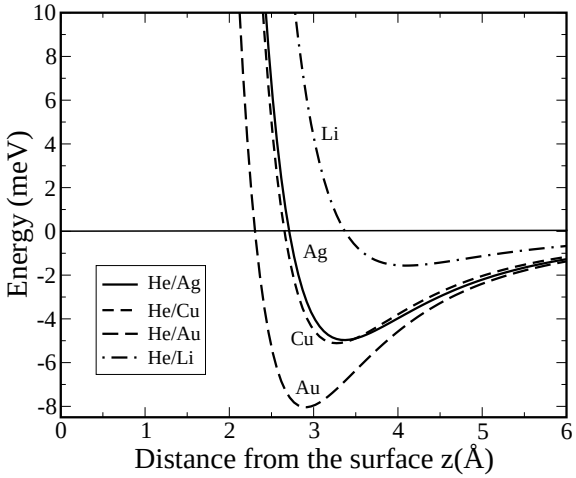

Figure 10: Interaction potential of He with different jellium surfaces as a function of the distance from the jellium edge. The jellium electronic densities correspond to the noble metals Ag, Cu and Au and the simple metal Li, respectively (after [51]).

theory [51]. It is obvious that the physisorption minimum for He is rather far away from the surface ($\gtrsim$ 3 Å) and shallow (below 10 meV).

In contrast to physisorption, chemisorption corresponds to the creation of a true chemical bond between adsorbate and substrate. This means that the electronic structure of both the substrate and adsorbate are strongly perturbed by the interaction. As far as the energy gain upon adsorption is concerned, the adsorption or bonding energy, there can be a delicate balancing between different opposing effects so that it is not always easy to develop a true understanding. We will discuss here some basic mechanisms, namely ionic and covalent bonding. Again we will use DFT calculations addressing adsorption on a jellium surface in order to illustrate the main trends.

In order to identify the energetic contributions to chemisorption within density functional theory, we regroup the different energetic terms in the total energy expression (15) yielding

$$\begin{aligned} E_{\rm tot} &= \sum_{i=1}^{N} \varepsilon_i + E_{\rm xc}[n] - \int v_{\rm xc}(\mathbf{r}) n(\mathbf{r}) d^3\mathbf{r} - V_{\rm H} + V_{\rm nucl-nucl} \\ &= \sum_{i=1}^{N} \varepsilon_i + E_{\rm xc}[n] - \int v_{\rm eff}(\mathbf{r}) n(\mathbf{r}) d^3\mathbf{r} + E_{\rm es} \ . \end{aligned} \tag{25}$$

Here we have included the interaction between the nuclei or ion cores $V_{\rm nucl-nucl}$ (see Eq. 3) which acts as a renormalization constant in any electronic structure calculation so that $E_{\rm es}$ corresponds to the total electrostatic energy of the system. The sum $\sum \varepsilon_i = E_{\rm bs}$ is the band-structure term. The adsorption energy is given by the energy difference between the energies of the separate constituents and the interacting system

$$E_{\rm ads} = (E_{\rm tot}({\rm substrate}) + E_{\rm tot}({\rm atom})) - E_{\rm tot}({\rm adatom/substrate}) \ . \tag{26}$$

Here the adsorption energy is positive if the adsorption is stable. However, there is no consistency in the literature as far as the sign of the adsorption energy is concerned. There are several

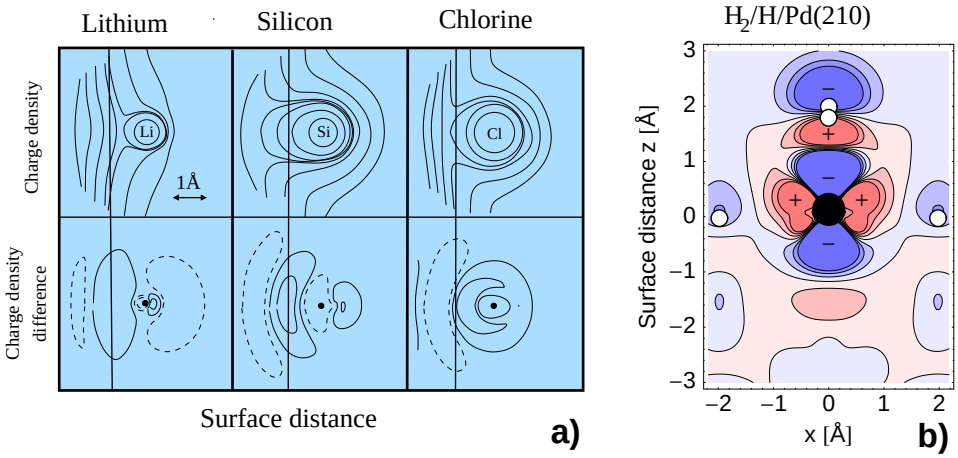

Figure 11: Charge density and charge density difference plots of chemisorption systems calculated with DFT methods. a) Contours of constant charge density calculated for Li, Si and Cl adsorbed on a high-density jellium substrate. The solid vertical line indicates the jellium edge. Upper panel: Total charge density of states; lower panel: charge density difference, broken lines correspond to charge depletion (after [52]). b) Charge density difference plot of H_2 adsorbed on the top site above a Pd atom of a H(1×1)/Pd(210) surface. Regions of charge depletion are denoted by a minus sign (after [23]).

terms contributing to the total energy and consequently to the energy difference. Most often, the chemical interaction is analyzed in terms of the electronic band structure term and electrostatic contributions.

The upper panel of Fig. 11a shows contours of constant charge density calculated for Li, Si and Cl adsorbed on a high-density jellium substrate representative for Al[52]. Although there are some differences, these plots still look rather similar for the three adsorbates. It is much more instructive to look at the charge density difference between the interacting system and the superposition of the bare atom and the substrate which corresponds to the adsorption induced charge density redistribution and rehybridization. These plots exhibit regions of charge depletion and charge accumulation indicating the charge transfer upon the adsorption.

The lower panel of Fig. 11a illustrates that there is charge transfer from the vacuum side of the Li adatom towards the metal while for Cl there is a significant charge transfer from the substrate to the adsorbate. This charge flow is caused by the difference in the electronegativity between the metal and the adsorbates leading to positive ionic chemisorption in the case of Li and to negative ionic chemisorption in the case of Cl. The adsorbed silicon atom, on the other hand, shows charge transfer from the region close to the nucleus to both the vacuum and the bond region. Such a charge accumulation in the bond region is typical for the formation of a covalent bond with the maximum charge density in between the two bonding partners.

For realistic systems, charge density difference plots can reveal much more details of the interaction between substrate and adsorbate. Figure Fig. 11b shows the adsorption induced charge redistribution upon the adsorption of molecular hydrogen on top of a Pd atom of a hydrogen covered

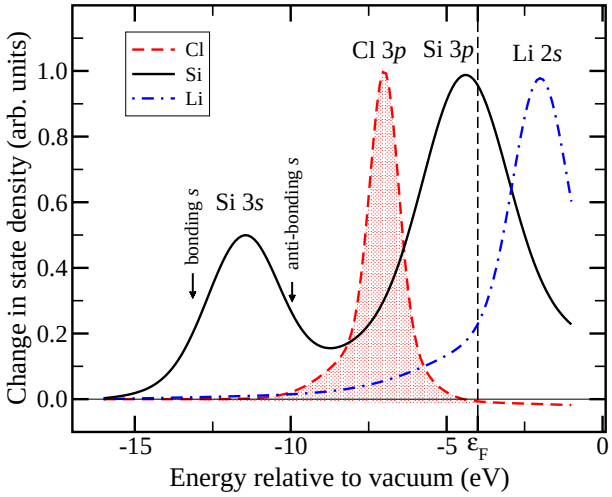

Figure 12: Change of the density of states upon the adsorption of Cl, Si and Li on jellium with an electron density corresponding to Al (after [52]).

H(1×1)/Pd(210) surface [23, 53]. The main bonding occurs via the $d_{3z^2-r^2}$ orbital of the Pd atom which can already be deduced from the pattern of the charge redistribution. Furthermore, the strong polarization of the adsorbed H_2 molecule is visible leading to a significant reduction of the work function [23, 53].

In addition to the spatial information about the charge redistribution upon adsorption, the change in the density of states can give insight into the delicate energetic balance between band-structure and electrostatic contributions to the chemical bonding. The change of the density of states upon the adsorption of Li, Si and Cl is plotted in Fig. 12. There are several peaks that correspond to adatom levels which have been shifted and broadened due to the interaction with the jellium substrate.

The Cl $3p$ derived state is basically fully occupied since it is almost entirely below ε_F indicating the negative ionic chemisorption, whereas the Li $2s$ derived state which is singly occupied in the free atom lies primarily above the Fermi energy ε_F. This confirms the charge transfer from the Li atom to the substrate and hence the positive ionic chemisorption. The density of states of Si adsorbed on jellium shows two prominent peaks which can be associated with the Si $3s$ and $3p$ atomic levels. The Si $3p$ derived state is only half-filled. Typically the lower part of such a resonance adds charge to the bond region while the upper parts substract charge from this region [1]. The lower parts can therefore be associated with a bonding contribution while the upper parts have an antibonding character. Hence a half-filled resonance level corresponds to a covalent bonding interaction in weak chemisorption cases. These considerations also explain why d-band metals with a half-filled d band show the largest cohesive and surface energies (see Fig. 6). For Cl adsorption, both the bonding and antibonding contributions are occupied. In this case it is the electrostatic attraction between the Cl core and the transferred electron that stabilizes the adsorption.

In order to illustrate the possible complexity of the molecule-surface interaction, we will use the dissociative adsorption of methanol on Cu(110) as an example [54]. The interaction of methanol

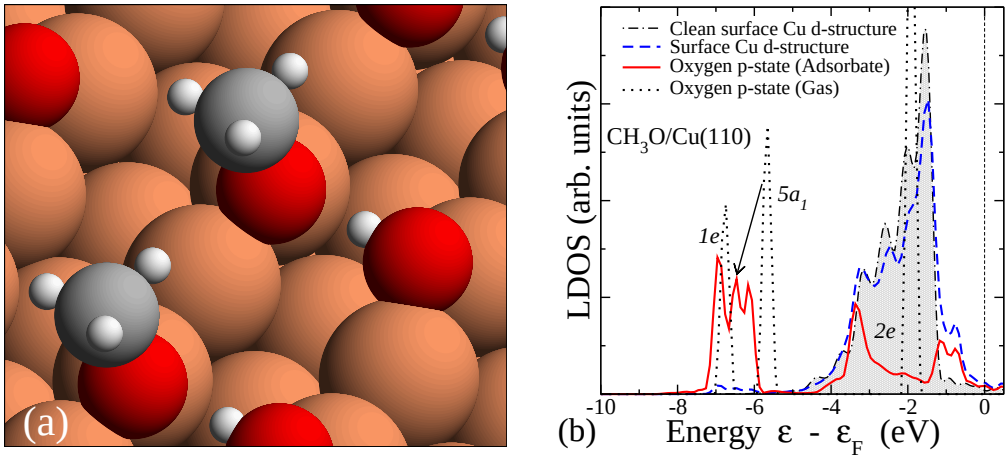

Figure 13: Dissociative adsorption of methanol (CH_3OH) on a oxygen covered Cu(110) surface. a) Geometry of neighboring methoxy and hydroxyl after the spontaneous methanol hydroxyl bond decomposition on O/Cu(110). b) Projected local density of states (LDOS) of the oxygen atom of methoxy on Cu(110). The methoxy orbitals are strongly perturbed due to the interaction with the Cu substrate (after [54]).

with copper surfaces is of strong current interest in the context of the catalytic oxidation and synthesis of methanol. On oxygen-covered Cu(110), methanol (CH_3OH) dissociates spontaneously into methoxy (CH_3O) and hydroxyl (OH, see Fig. 13a). The methoxy radical is strongly interacting with the copper surface. The $2e$ orbital which corresponds to a nonbonding π orbital on oxygen is only partially filled in the gas-phase [55]. As Fig. 13b shows, this $2e$ orbital is significantly broadened by the direct coupling to the Cu d-states which causes the high adsorption energy. The oxygen p_x and p_y ($1e$) states are no longer degenerate, but split by the reduced symmetry at the adsorption site. Furthermore, the p_z ($5a_1$) orbital is shifted down by about 2 eV between the two $1e$-derived peaks.

Such a significant rearrangement of the electronic structure is always indicative of a strong interaction between adsorbate and substrate. This is also reflected in the relatively large adsorption energy of almost 3 eV [54]. However, a strong interaction is not always associated with a large binding energy. For example, formaldehyde (CH_2O) adsorbed above the short-bridge site of Cu(110) also exhibits a considerable rehybridization of its levels upon adsorption. Still, it is only bound by 0.6 eV to Cu(110). This is due to the fact that the adsorbed formaldehyde is significantly distorted so that the energy gain upon adsorption is compensated to a large extent by the energetic cost of the deformation of the molecule [54].

6 Conclusions

In this short introduction into theoretical surface science I have given a brief overview over the main theoretical tools to address surface problems from a microscopic point of view. Some illustrative examples have been used in order to discuss the main mechanisms underlying the structure of

surfaces and the interaction of atoms and molecules with surfaces. Of course, surface science is a much broader field that also covers, e.g., phase transitions at surfaces or the dynamics and kinetics of gas-surface interactions and reactions at surfaces. A decription of these processes requires further theoretical methods and tools. However, the combination of methods such as molecular dynamics simulations or thermodynamical approaches with information from electronic structure calculations permits to address complex stuctures and processes at surfaces from first principles, even on rather long length and time scales. This makes theoretical surface science to a very active and fruitful research field in close collaboration with the experiment allowing detailed insights into the microscopic world at surfaces.

References

[1] A. Groß, *Theoretical surface science – A microscopic perspective*, Springer, Berlin, 2002.

[2] G. Binnig, H. Rohrer, C. Gerber, and E. Weibel, Phys. Rev. Lett. **49**, 57 (1982).

[3] A. Groß, Surf. Sci. **500**, 347 (2002).

[4] M. Born and J. R. Oppenheimer, Ann. Phys. **84**, 457 (1927).

[5] W. Kohn, Rev. Mod. Phys. **71**, 1253 (1999).

[6] N. W. Ashcroft and N. D. Mermin, *Solid State Physics*, Saunders College, Philadelphia, 1976.

[7] C. Kittel, *Introduction to Solid State Physics*, John Wiley & Sons, New York, sixth edition, 1986.

[8] J. L. Whitten and H. Yang, Surf. Sci. Rep. **24**, 55 (1996).

[9] P. Hohenberg and W. Kohn, Phys. Rev. **136**, B864 (1964).

[10] W. Kohn and L. Sham, Phys. Rev. **140**, A1133 (1965).

[11] E. H. Lieb, Rev. Mod. Phys. **53**, 603 (1981).

[12] B. J. Zhou, V. L. Ligneres, and E. A. Carter, J. Chem. Phys. **122**, 044103 (2005).

[13] M. C. Payne, M. P. Teter, D. C. Allan, T. A. Arias, and J. D. Joannopoulos, Rev. Mod. Phys. **64**, 1045 (1992).

[14] B. Hammer, M. Scheffler, K. Jacobsen, and J. Nørskov, Phys. Rev. Lett. **73**, 1400 (1994).

[15] J. P. Perdew et al., Phys. Rev. B **46**, 6671 (1992).

[16] B. Hammer, L. B. Hansen, and J. K. Nørskov, Phys. Rev. B **59**, 7413 (1999).

[17] P. J. Feibelman et al., J. Phys. Chem. B **105**, 4018 (2001).

[18] N. D. Lang and W. Kohn, Phys. Rev. B **1**, 4555 (1970).

[19] N. D. Lang and W. Kohn, Phys. Rev. B **3**, 1215 (1971).

[20] M. Mavrikakis, B. Hammer, and J. K. Nørskov, Phys. Rev. Lett. **81**, 2819 (1998).

[21] A. Roudgar and A. Groß, Phys. Rev. B **67**, 033409 (2003).

[22] A. Roudgar and A. Groß, J. Electroanal. Chem. **548**, 121 (2003).

[23] M. Lischka and A. Groß, Phys. Rev. B **65**, 075420 (2002).

[24] B. Hammer and J. K. Nørskov, Surf. Sci. **343**, 211 (1995).

[25] B. Hammer and J. K. Nørskov, Nature **376**, 238 (1995).

[26] K. Fukui, Science **218**, 747 (1982).

[27] R. Hoffmann, Rev. Mod. Phys. **60**, 601 (1988).

[28] B. Hammer, O. H. Nielsen, and J. K. Nørskov, Catal. Lett. **46**, 31 (1997).

[29] V. Pallassana, M. Neurock, L. B. Hansen, B. Hammer, and J. K. Nørskov, Phys. Rev. B **60**, 6146 (1999).

[30] S. Dahl et al., Phys. Rev. Lett. **83**, 1814 (1999).

[31] S. Dahl, E. Törnqvist, and I. Chorkendorff, J. Catal. **192**, 381 (2000).

[32] M. Methfessel, D. Hennig, and M. Scheffler, Phys. Rev. B **46**, 4816 (1992).

[33] L. Vitos, A. V. Ruban, H. L. Skriver, and J. Kollár, Surf. Sci. **411**, 186 (1998).

[34] R. Smoluchowski, Phys. Rev. **60**, 661 (1941).

[35] S. Sakong and A. Groß, unpublished.

[36] W. R. Tyson and W. A. Miller, Surf. Sci. **62**, 267 (1977).

[37] S. Lindgren, L. Walldén, J. Rundgren, and P. Westrin, Phys. Rev. B **29**, 576 (1984).

[38] S. Walter, V. Blum, L. Hammer, K. Heinz, and M. Giesen, Surf. Sci. **458**, 155 (2000).

[39] S. Liem, G. Kresse, and J. Clarke, Surf. Sci. **415**, 194 (1998).

[40] D. L. Adams, H. B. Nielsen, and J. N. Andersen, Surf. Sci. **128**, 294 (1983).

[41] J. Northrup and S. Froyen, Phys. Rev. B **50**, 2015 (1994).

[42] N. Moll, A. Kley, E. Pehlke, and M. Scheffler, Phys. Rev. B **54**, 8844 (1996).

[43] X. G. Wang, A. Chaka, and M. Scheffler, Phys. Rev. Lett. **84**, 3650 (2000).

[44] C. Verdozzi, D. R. Jennison, P. A. Schultz, and M. P. Sears, Phys. Rev. Lett. **82**, 799 (1999).

[45] R. Di Felice and J. E. Northrup, Phys. Rev. B **60**, R16287 (1999).

[46] I. Batyrev, A. Alavi, and M. W. Finnis, Faraday Discuss. **114**, 33 (1999).

[47] P. Guénard, G. Renaud, A. Barbier, and M. Gautier-Soyer, Surf. Rev. Lett. **5**, 321 (1998).

[48] J. Toofan and P. R. Watson, Surf. Sci. **401**, 162 (1998).

[49] E. Soares, M. A. Van Hove, C. F. Walters, and K. F. McCarty, Phys. Rev. B **65**, 195405 (2002).

[50] E. Zaremba and W. Kohn, Phys. Rev. B **13**, 2270 (1976).

[51] E. Zaremba and W. Kohn, Phys. Rev. B **15**, 1769 (1977).

[52] N. D. Lang and A. Williams, Phys. Rev. B **18**, 616 (1978).

[53] P. K. Schmidt et al., Phys. Rev. Lett. **87**, 096103 (2001).

[54] S. Sakong and A. Groß, J. Catal. **231**, 420 (2005).

[55] C. F. Jackels, J. Chem. Phys. **82**, 311 (1985).